



Spectral dynamics of soft X-ray emission in dual-laser-produced medium-Z plasma

Hayato Ohashi¹ · Hiroyuki Hara² · Goki Arai² · Tadashi Hatano³ · Takeo Ejima³ · Chihiro Suzuki⁴ · Shinichi Namba⁵ · Akira Sasaki⁶ · Masaharu Nishikino⁶ · Gerry O'Sullivan⁷ · Takeshi Higashiguchi²

Received: 2 July 2018 / Accepted: 30 August 2018 / Published online: 5 September 2018
© Springer-Verlag GmbH Germany, part of Springer Nature 2018

Abstract

Laser-produced medium element plasma sources are being considered as strong candidates for in vivo photographic imaging of biological samples in laboratory-scale water-window soft X-ray microscopes. We explored spectral changes in the emission from dual-laser-produced zirconium (Zr) plasmas in the water-window soft X-ray spectral region. The emission was enhanced at a delay time of 5 ns between the pre- and main-laser pulses and found to possess a source size of $38 \mu\text{m} \times 68 \mu\text{m}$ very similar to that obtained without any pre-pulse. We also investigated the decrease in emission observed at longer delay times, in the context of the collisional-radiative (CR) model-calculated absorption coefficient.

1 Introduction

The hot, dense plasmas produced by 1- μm solid-state laser pulses generate efficient, bright short wavelength emission in the vacuum ultraviolet (VUV), extreme ultraviolet (EUV), and soft X-ray spectral regions, as the result

of transitions in highly charged ions [1, 2]. The emission from such laser-produced plasmas can be applied for specific applications, such as X-ray absorption fine structure measurements [3], ablation [4], lithography [5], and biological imaging [6]. The spectral structure observed in higher atomic number (higher-Z) element plasmas, such as those of tin (Sn), xenon (Xe), gadolinium (Gd), and bismuth (Bi), can show a dramatic difference from strong line emitting lower atomic number (lower-Z) element plasmas [7–9], such as carbon and nitrogen plasmas, and be dominated instead by continuum emission from unresolved transition arrays (UTAs) [10–20]. Plasmas of the higher Z elements Sn and Gd, which are candidates for the next-generation semiconductor lithography light sources, produce strong resonant emission due to $4p-4d$ and $4d-4f$ transitions at 13.5 nm and 6.7 nm, within wavelength bandwidths of 2% and 0.6%, respectively [21–24]. The resulting line emission from adjacent ion stages overlaps to yield an intense UTA emission in their spectra. The in-band high-energy emission is thus attributable to hundreds of thousands of near-degenerate resonance lines lying within a narrow wavelength region [21, 22]. Generally speaking, the spectral profiles of the emission are determined by the balance between the emissivity and the self-absorption (opacity) in the plasmas as they expand into the vacuum. In addition, the 1- μm laser-produced plasmas are optically thick for higher Z element targets, such as Sn, Gd, and Bi compared to for lower Z element targets of C and N. Although the output flux from the

✉ Hayato Ohashi
ohashi@las.u-toyama.ac.jp

Takeshi Higashiguchi
higashi@cc.utsunomiya-u.ac.jp

¹ Institute of Liberal Arts and Sciences, University of Toyama, Toyama 930-8555, Japan

² Department of Electrical and Electronic Engineering, Faculty of Engineering, Utsunomiya University, Yoto 7-1-2, Utsunomiya, Tochigi 321-8585, Japan

³ Institute of Multidisciplinary Research for Advanced Materials, Tohoku University, 2-1-1, Katahira, Aoba-ku, Sendai 980-8577, Japan

⁴ National Institute for Fusion Science (NIFS), National Institutes of Natural Science (NINS), Toki, Gifu 509-5292, Japan

⁵ Graduate School of Engineering, Hiroshima University, 1-4-1 Kagamiyama, Higashihiroshima, Hiroshima 739-8527, Japan

⁶ Kansai Photon Science Institute, National Institutes for Quantum and Radiological Science and Technology (QST), Kizugawa, Kyoto 619-0215, Japan

⁷ School of Physics, University College Dublin, Belfield, Dublin 4, Ireland

UTAs is generally strong for high- Z plasmas, the effects of self-absorption in such plasmas are also large especially if compared to lower Z plasmas [25, 26].

One of the most important applications at shorter wavelengths is in vivo biological imaging in the water-window soft X-ray spectral region, which lies between an oxygen K-edge (O_K -edge) at 2.3 nm and the carbon K-edge (C_K -edge) at 4.4 nm, and which is the focus of much interest because of its potential for high-resolution biomedical research. The selection of target elements is, therefore, critical to maximize emission to develop the most efficient light sources for soft X-ray microscopy and soft X-ray tomography. According to the quasi-Moseley's law [27], plasmas of higher Z elements are expected to produce high output flux, which originates from unresolved spectral structure due to $n = 4 - n = 4$ transitions. It predicts that Bi is one of the most promising elements for use in an efficient water-window soft X-ray light source [19]. However, higher electron temperatures, which correspond to higher laser intensity (laser power density), in the 400–600 eV range are required to produce highly charged ions as the emitters for such a high- Z plasma source [19]. Recently, it has been shown that plasmas of medium- Z elements, such as zirconium (Zr) and molybdenum (Mo), produce similar output flux at relatively lower electron temperatures of 200–400 eV [28–30]. In fact, the optimum electron temperature was observed to be about 250 eV under optically thin conditions in discharge-produced plasmas [31]. In addition, the spectral behavior of water-window soft X-ray emission from a Mo plasma has also been observed from dual-pulse laser-produced plasmas [32]. However, to date, no comparison has been made between the observed spectra and the calculated emissivity and opacity for Zr plasmas for water-window soft X-ray microscopy sources, especially the self-absorption (opacity) effect. To observe the absorption effects, the optical thickness, which is related to the electron and ion densities, and the length of the plasma through which the radiation passes, should be controlled. The optical thickness is determined by the initial density of the target [14, 18], the thickness of the target [25], the pulse duration [33, 34] and wavelength of the laser pulse [12, 17, 20], and the irradiation scheme, i.e., whether single- or dual-laser-pulse irradiation is used [14, 18, 32, 35]. The dual-laser-pulse irradiation technique is useful in a controlled way to influence the behavior of the opacity of the expanding plasma, here provided by the pre-plasma. We, therefore, focus here on changes in spectral behavior with source size by changing the delay time in a dual-pulse laser irradiation scheme.

In this paper, we explore spectral changes of the emission in the water-window soft X-ray spectral region. The emission is slightly enhanced at a delay time of 5 ns, while the source size is essentially similar to that obtained without any pre-pulse. We also discuss the effects of

self-absorption based on the results of opacity (absorption coefficient) calculations with a collisional-radiative (CR) model.

2 Experimental apparatus

The spectral behavior of Zr plasma emission under dual-pulse laser irradiation was observed using the experimental apparatus described previously in Ref. [32]. The experiment was performed using two Q -switched Nd:YAG lasers in which the pulse durations of the pre-pulse and the main pulse had the same value of 150 ps at a wavelength of 1064 nm. The pulse energies of the pre-pulse and the main pulse were 20 and 200 mJ, respectively. The pre-pulse was loosely focused to produce a large volume pre-plasma before irradiating with the main pulse after a variable pulse delay. The laser intensity of the pre-pulse was 3.5×10^{10} W/cm² with a focal spot diameter of 700 μ m, and the main pulse was tightly focused to a maximum intensity of 1.1×10^{14} W/cm² at a focal spot diameter of 40 μ m. We define the delay time as the difference between the intensity peaks of the two different laser pulses. The laser systems were synchronized by a trigger pulse oscillator, which controlled the timing of the flash lamps and Q -switching. The pulse-to-pulse stability (jitter) evaluated over many shots was determined to have standard deviations of 0.2 ns in the present experiments. The pre-pulse and main pulse were focused on to a $_{40}\text{Zr}$ planar target, through plano-convex lenses with focal lengths of 25 cm. The pre-pulse laser irradiated the target at an incident angle of 60° with respect to the main pulse laser axis. The resulting pre-pulse laser power density was sufficient to create a lowly ionized plasma but not enough to obtain emission in the soft X-ray spectral region.

The plasmas were formed along the optical axis of the main-laser pulse on the normal of the target. A flat-field grazing incidence spectrometer with a variable-line-spacing 2400 grooves/mm grating was positioned at 30° with respect to the incident main laser axis. Spectra were recorded by a thermoelectrically cooled back-illuminated X-ray CCD camera. The spectra were obtained over the spectral range from 1 to 7 nm. The uncertainty of the present wavelength calibration is estimated to be 0.01 nm. The relative response of the grating and the X-ray CCD camera were calibrated by synchrotron radiation with a reflectometer installed at the BL-11D beamline of the Photon Factory (PF) at KEK [36]. An X-ray pinhole camera with a 15- μ m pinhole was used to determine the spatial extent of the soft X-ray emission and was positioned at 90° with respect to the main laser axis. A 200-nm-thick Ti filter was inserted between the pinhole and an X-ray CCD camera to transmit the water-window soft X-ray spectral region longer than 2.9 nm.

3 Experimental results and discussion

The spectral changes obtained by changing the delay time between the pre-pulse and the main pulse is shown in Fig. 1a. The emission spectrum from the Zr plasma without the pre-pulse (single-pulse irradiation) is observed in Fig. 1a in Ref. [30]. The energy stability of the main-laser pulse was $\pm 5\%$ at the pulse energy of 220 mJ in the present results. At one delay time, we recorded five spectra, and we averaged the spectra using the recorded spectra at each delay time. After taking various delay time of each 2-ns delay, we map Fig. 1a. The spectral intensity was normalized to the spectral intensity measured without the pre-pulse (i.e., single-main-pulse irradiation). The emission intensity is clearly enhanced at delay times of 4–8 ns in the 1.7–7-nm spectral region, and reduced at delay times of 0–3 and 22–50 ns from 1.8 to 4 nm. In Fig. 1b, the changes

in the spectra at delay times of 5 and 30 ns are shown. The emission at 2.1 nm was increased by a factor of +18% at the 5-ns delay and the 3.1-nm emission was decreased by -15% at the delay time of 30 ns. To understand this behavior, we calculated the radiation coefficient (emissivity) and the absorption coefficient (opacity) by the collisional-radiative (CR) model [37] and the results are shown in Fig. 2a, b, respectively. In Refs. [37] and [38], the CR model is described in detail. In Fig. 2a, the strong radiation coefficient is predicted maximized in the 2–2.4-nm wavelength region at an electron temperature higher than 200 eV. Strong discrete spectral structure in the water-window soft X-ray spectral region can be attributed to overlapping lines of $3d^n - 3d^{n-1}4f$ ($n = 3 - n = 4$, $\Delta n = 1$) transitions. The transitions of the type $3p - 4d$, which originate from ion stages with an outermost $3p$ subshell, appear at shorter wavelengths, while at longer wavelengths, distinct line groups attributable to $3d^n - 3d^{n-1}4p$

Fig. 1 **a** Normalized Zr laser-produced plasma spectra for different delay times between the pre- and main pulses, compared to the spectrum obtained with the single main pulse and **b** differences of emission intensity at delay times of 5 and 30 ns. At one delay time, we recorded five spectra, and we averaged the spectra using the recorded spectra at each delay time

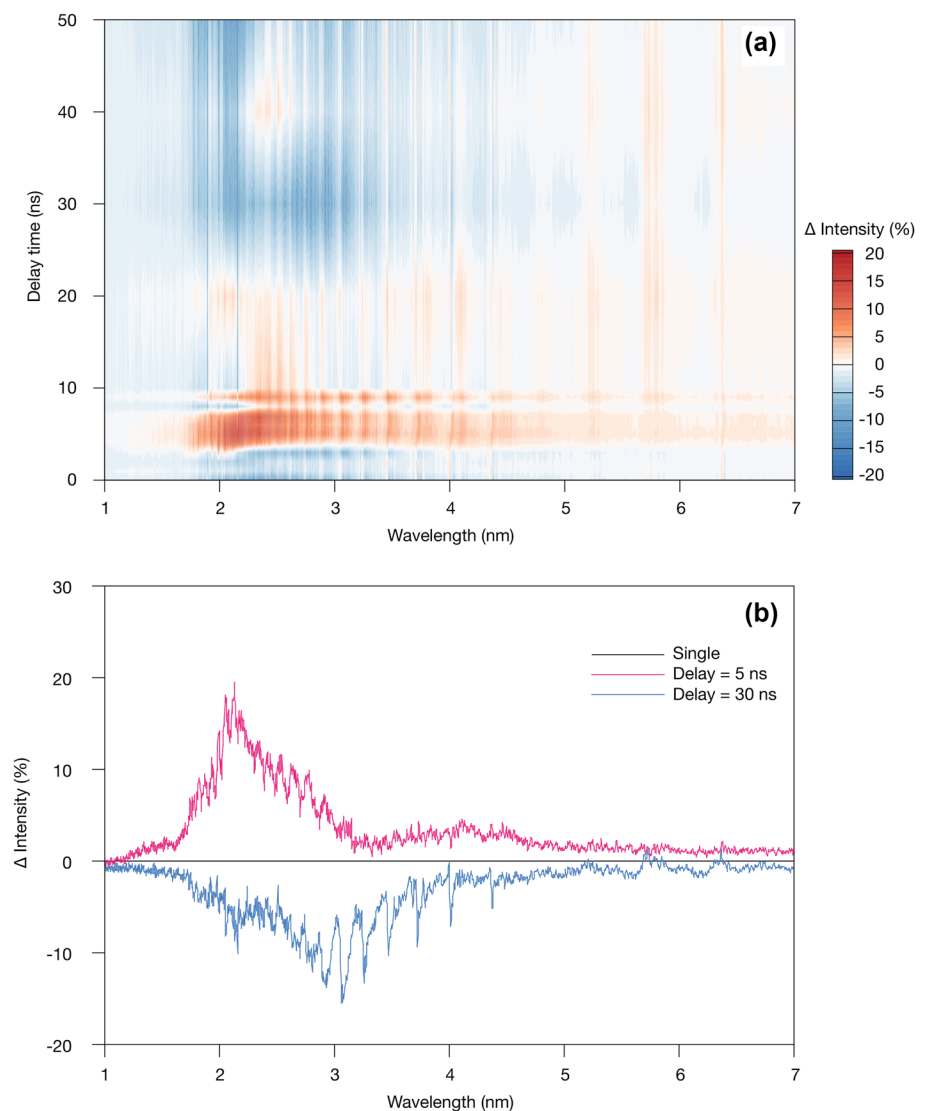
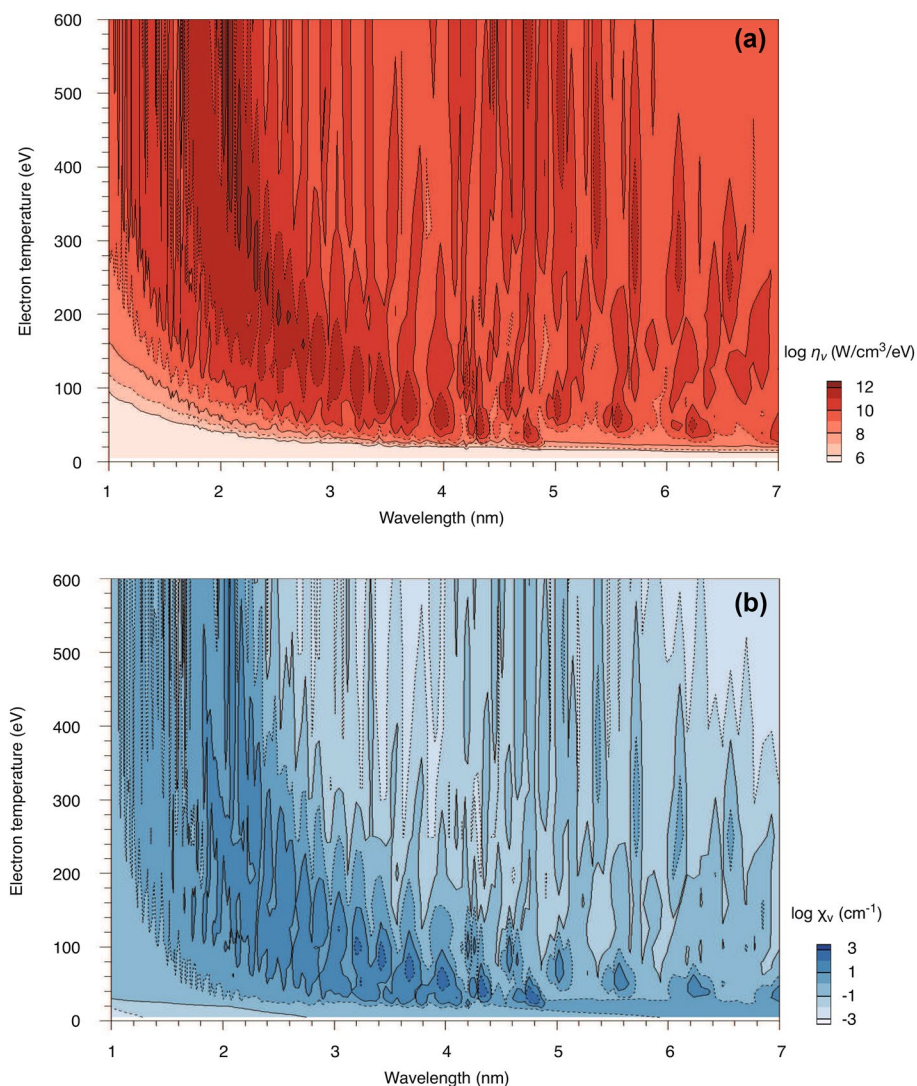


Fig. 2 Calculated electron temperature dependence of the radiation emissivity coefficient η_v (a) and absorption coefficient χ_v (b) of Zr at an electron density of $1 \times 10^{20} \text{ cm}^{-3}$ obtained using the CR model



transitions appear. Satellite lines from transitions of the type $3d^{n-1}4s - 3d^{n-2}4s4f$ also contribute in the water-window soft X-ray region lying on the low energy side of the resonant $3d - 4f$ transitions. The upper $3d^{n-2}4s4f$ configurations are efficiently populated by dielectronic recombination and the radiative decay rate for individual levels is typically around 5% of the autoionizing rate, so that they contribute significantly to the overall emission [28]. On the other hand, the absorption coefficient, which determines the opacity effects, was calculated to be low as shown in Fig. 2b. Self-absorption effects are, therefore, expected to be low in Zr plasmas in the 1.8 – 5 nm spectral region. In fact, the overall emission flux in the water-window soft X-ray spectral region was found to be almost constant for different delay times, as shown in Fig. 3. According to Figs. 1 and 2, the emission was increased at the delay time of 5 ns, which is corresponded to the electron temperature of 300 eV in Figs. 1a and 2a. In addition, the decreased emission at the delay time of

30 ns is from the low electron temperature around 100 eV in Figs. 1b and 2b due to the expanding plasma into the vacuum. This result was consistent with the predictions for the CR model-calculated absorption coefficient. This means that self-absorption is expected to be lower compared to that observed in higher Z plasmas [25, 26, 32, 39]. According to the atomic calculation with the CR model, the absorption coefficient of Zr, as medium-Z element, was evaluated to be 7.3 cm^{-1} for 2.1-nm emission at an electron temperature of 300 eV, significantly smaller than the value of 15.9 cm^{-1} obtained for 4-nm emission at the electron temperature of 500 eV for Bi, as high-Z element, at an electron density of $1 \times 10^{20} \text{ cm}^{-3}$. The emission flux was about 1×10^{14} photons/sr [30]. Since the availability of detailed spectral data for Zr ions is limited, the present results show that it is important to improve both the energy level and rate-coefficient information for detailed CR modeling.

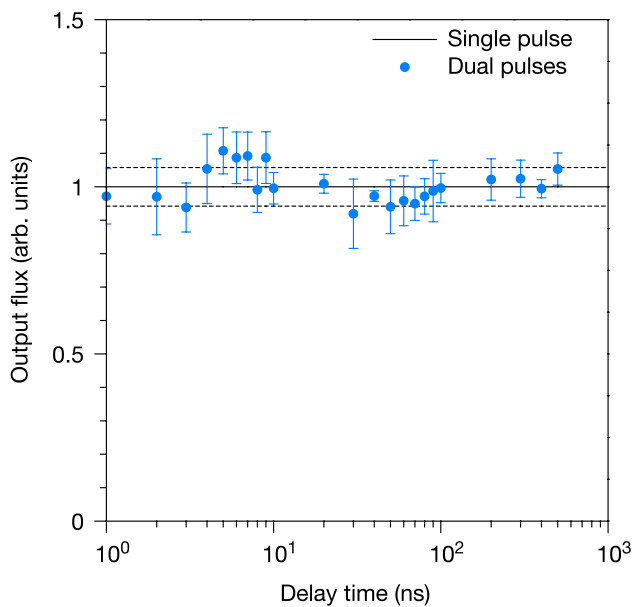


Fig. 3 Delay time dependence of the output flux in the water-window soft X-ray spectral region

Slight increase of the emission at the wavelengths of 2.4 and 6.6 nm was observed. However, it is difficult to understand this spectral behavior. Then, we need the radiation hydrodynamic simulation, coupling with the atomic code calculation in near future. In the radiation hydrodynamic simulation, it is difficult to compare the experimental results with the time-resolved simulations for the spectra, because the calculation of the equation of states (EOS) for Zr is very difficult. In fact, there are many proposals and methods to calculate of the EOS. This equation is very important to connect the energy flow at different positions and the states of the Zr. Then, we remain some problems before the radiation

hydrodynamic simulation for Zr to compare the experimental results.

Since high brightness and a small source size are essential for microscopy, we also studied the source sizes obtained, as the size of the water-window soft X-ray emission volume might be expected to increase due to plasma formation by the pre-pulse. The emission has been shown to be enhanced at the delay time of 5 ns, but the source size of $38 \mu\text{m} \times 68 \mu\text{m}$ in Fig. 4b is very similar to that of $33 \mu\text{m} \times 71 \mu\text{m}$, obtained without the pre-pulse, as shown in Fig. 4a. The extent of the source size along the incident laser axis is determined by plasma expansion and was seen to be almost constant for different delay times (not shown). The resulting emission is then weakly absorbed in the expanding plasma. As a result, the integrated output flux in the water-window soft X-ray region and the source size were almost constant and independent of the delay time between the two laser pulses although the detailed spectral behavior changes as is clearly shown in Fig. 1a, b.

4 Summary

In summary, we have demonstrated changes in the spectral emission in the water-window soft X-ray spectral region under dual-laser-pulse irradiation. The overall emission was enhanced at a delay time of 5 ns, and the emitting source size of $38 \mu\text{m} \times 68 \mu\text{m}$ was similar to that of $33 \mu\text{m} \times 71 \mu\text{m}$ obtained without the pre-pulse. We have also discussed the decrease of emission observed at longer interpulse delays and shown it to be consistent with the predictions for the CR model-calculated absorption coefficient. The Zr plasma source is one of the candidates for imaging of in vivo biological samples in the water-window soft X-ray spectral region.

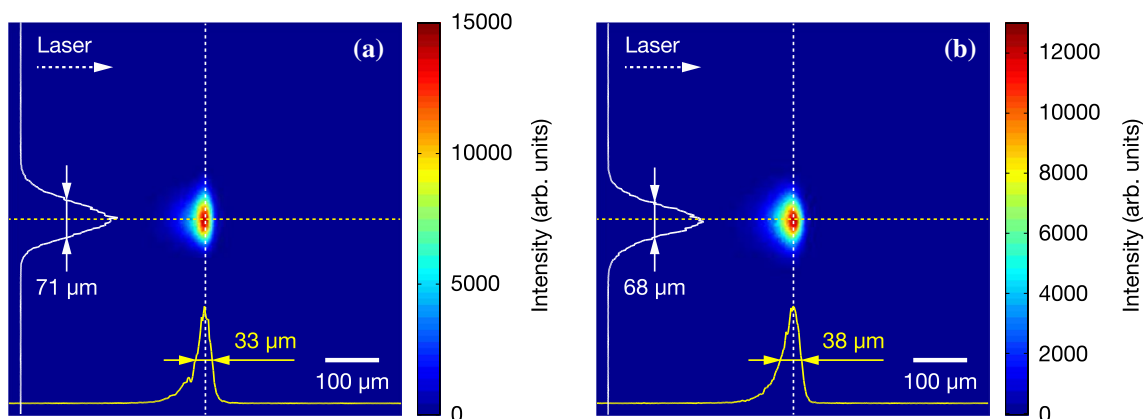


Fig. 4 Time-integrated pinhole images of soft X-ray emission without the pre-pulse (a) and with the pre-pulse at pulse separation times of 5 ns (b)

Acknowledgements This work was supported by JSPS (Japan Society for the Promotion of Science) KAKENHI, Grant-in-Aid for Scientific Research (B) Grant no. JP15H03570, Grant-in-Aid for Young Scientists (B) Grant no. JP15K17728, Grant-in-Aid for JSPS Research Fellow Grant no. 17J08957, and the JSPS Bilateral Joint Research Project. This work was also performed under the Cooperative Research Program of “Network Joint Research Center for Materials and Devices” (under contract subject “20183037”). Measurements of the grating efficiency and the response of the X-ray CCD camera were performed with the approval of the Photon Factory Program Advisory Committee (proposal no. 2015G667). The UCD group was supported by the Science Foundation Ireland International Co-operation Strategic Award 13/ISCA/2846.

References

- I.C.E. Turcu, J.B. Dance, *X-Rays From Laser Plasmas: Generation and Applications* (Wiley, West Sussex, England, 1999), Chap. 4
- D.T. Attwood, *Soft X-rays and extreme ultraviolet radiation*. (Cambridge University Press, Cambridge, 2000), Chap. 6
- C. Peth, F. Barkusky, K. Mann, *J. Phys. D* **41**, 105202 (2008)
- T. Makimura, S. Mitani, Y. Kenmotsu, K. Murakami, M. Mori, K. Kondo, *Appl. Phys. Lett.* **86**, 103111 (2005)
- C.W. Gwyn, R. Stulen, D. Sweeney, D. Attwood, *J. Vac. Sci. Technol., B* **16**, 3142 (1998)
- P.A.C. Takman, H. Stollberg, G.A. Johansson, A. Holmberg, M. Lindblom, H.M. Hertz, *J. Microsc.* **226**, 175 (2007)
- P.A.C. Jansson, U. Vogt, H.M. Hertz, *Rev. Sci. Instrum.* **76**, 043503 (2005)
- H. Legall, G. Blobel, H. Stiel, W. Sandner, C. Seim, P. Takman, D.H. Martz, M. Selin, U. Vogt, H.M. Hertz, D. Esser, H. Sipma, J. Luttmann, M. Höfer, H.D. Hoffmann, S. Yulin, T. Feigl, S. Rehbein, P. Guttmann, G. Schneider, U. Wiesemann, M. Wirtz, W. Diete, *Opt. Express* **20**, 18362 (2012)
- T. Müller, Mey, J. Niemyer, K. Mann, *Opt. Express* **22**, 23489 (2014)
- G.-M. Zeng, H. Daido, T. Togawa, M. Nakatsuka, S. Nakai, H. Aritome, *J. Appl. Phys.* **69**, 7460 (1991)
- G. O’Sullivan, R. Faulkner, *Opt. Eng.* **33**, 3978 (1994)
- H. Tanaka, A. Matsumoto, K. Akinaga, A. Takahashi, T. Okada, *Appl. Phys. Lett.* **87**, 041503 (2005)
- T. Okuno, S. Fujioka, H. Nishimura, Y. Tao, K. Nagai, Q. Gu, N. Ueda, T. Ando, K. Nishihara, T. Norimatsu, N. Miyanaga, Y. Izawa, K. Mima, A. Sunahara, H. Furukawa, A. Sasaki, *Appl. Phys. Lett.* **88**, 161501 (2006)
- T. Higashiguchi, N. Dojyo, M. Hamada, W. Sasaki, S. Kubodera, *Appl. Phys. Lett.* **88**, 201503 (2006)
- Y. Ueno, G. Soumagne, A. Sumitani, A. Endo, T. Higashiguchi, *Appl. Phys. Lett.* **91**, 231501 (2007)
- Y. Tao, M.S. Tillack, S.S. Harilal, K.L. Sequoia, R.A. Burdt, F. Najmabadi, *Opt. Lett.* **32**, 1338 (2007)
- T. Otsuka, D. Kilbane, J. White, T. Higashiguchi, N. Yugami, T. Yatagai, W. Jiang, A. Endo, P. Dunne, G. O’Sullivan, *Appl. Phys. Lett.* **97**, 111503 (2010)
- T. Higashiguchi, T. Otsuka, N. Yugami, W. Jiang, A. Endo, B. Li, D. Kilbane, P. Dunne, G. O’Sullivan, *Appl. Phys. Lett.* **99**, 191502 (2011)
- T. Higashiguchi, T. Otsuka, N. Yugami, W. Jiang, A. Endo, B. Li, P. Dunne, G. O’Sullivan, *Appl. Phys. Lett.* **100**, 014103 (2012)
- T. Higashiguchi, B. Li, Y. Suzuki, M. Kawasaki, H. Ohashi, S. Torii, D. Nakamura, A. Takahashi, T. Okada, W. Jiang, T. Miura, A. Endo, P. Dunne, G. O’Sullivan, T. Makimura, *Opt. Express* **21**, 31837 (2013)
- G. O’Sullivan, P.K. Carroll, *J. Opt. Soc. Am.* **71**, 227 (1981)
- P.K. Carroll, G. O’Sullivan, *Phys. Rev. A* **25**, 275 (1982)
- S.S. Churilov, R.R. Kildiyarova, A.N. Ryabtsev, S.V. Sadovsky, *Phys. Scr.* **80**, 045303 (2009)
- D. Kilbane, *J. Phys. B* **44**, 165006 (2011)
- S. Fujioka, H. Nishimura, K. Nishihara, A. Sasaki, A. Sunahara, T. Okuno, N. Ueda, T. Ando, Y. Tao, Y. Shimada, K. Hashimoto, M. Yamaura, K. Shigemori, M. Nakai, K. Nagai, T. Norimatsu, T. Nishikawa, N. Miyanaga, Y. Izawa, K. Mima, *Phys. Rev. Lett.* **95**, 235004 (2005)
- C. O’Gorman, T. Otsuka, N. Yugami, W. Jiang, A. Endo, B. Li, T. Cummins, P. Dunne, E. Sokell, G. O’Sullivan, T. Higashiguchi, *Appl. Phys. Lett.* **100**, 141108 (2012)
- H. Ohashi, T. Higashiguchi, Y. Suzuki, G. Arai, Y. Otani, T. Yatagai, B. Li, P. Dunne, G. O’Sullivan, W. Jiang, A. Endo, H.A. Sakaue, D. Kato, I. Murakami, N. Tamura, S. Sudo, F. Koike, C. Suzuki, *Appl. Phys. Lett.* **104**, 234107 (2014)
- B. Li, T. Higashiguchi, T. Otsuka, W. Jiang, A. Endo, P. Dunne, G. O’Sullivan, *J. Phys. B* **45**, 245004 (2012)
- B. Li, T. Higashiguchi, T. Otsuka, W. Jiang, A. Endo, P. Dunne, G. O’Sullivan, *Appl. Phys. Lett.* **102**, 041117 (2013)
- T. Tamura, G. Arai, Y. Kondo, H. Hara, T. Hatano, T. Ejima, W. Jiang, C. Suzuki, G. O’Sullivan, T. Higashiguchi, *Opt. Lett.* **43**, 2042 (2018)
- H. Ohashi, H. Hara, B. Li, P. Dunne, G. O’Sullivan, A. Sasaki, C. Suzuki, N. Tamura, H. A. Sakaue, D. Kato, I. Murakami, T. Higashiguchi (**submitted**)
- R. Lokasani, G. Arai, Y. Kondo, H. Hara, T.-H. Dinh, T. Ejima, T. Hatano, W. Jiang, T. Makimura, B. Li, P. Dunne, G. O’Sullivan, T. Higashiguchi, *J. Limpouch, Appl. Phys. Lett.* **109**, 194103 (2016)
- T. Ando, S. Fujioka, H. Nishimura, N. Ueda, Y. Yasuda, K. Nagai, T. Norimatsu, M. Murakami, K. Nishihara, N. Miyanaga, Y. Izawa, K. Mima, *Appl. Phys. Lett.* **89**, 151501 (2006)
- T. Cummins, T. Otsuka, N. Yugami, W. Jiang, A. Endo, B. Li, C. O’Gorman, P. Dunne, E. Sokell, G. O’Sullivan, T. Higashiguchi, *Appl. Phys. Lett.* **100**, 061118 (2012)
- T. Higashiguchi, K. Kawasaki, W. Sasaki, S. Kubodera, *Appl. Phys. Lett.* **88**, 161502 (2006)
- T.-H. Dinh, Y. Kondo, T. Tamura, Y. Ono, H. Hara, H. Oikawa, Y. Yamamoto, M. Ishino, M. Nishikino, T. Makimura, P. Dunne, G. O’Sullivan, S. Ohta, K. Kitano, T. Ejima, T. Hatano, T. Higashiguchi, *Rev. Sci. Instrum.* **87**, 123106 (2016)
- A. Sasaki, *High Energy Density Phys.* **9**, 325 (2013)
- H. Hara, H. Ohashi, B. Li, P. Dunne, G. O’Sullivan, A. Sasaki, C. Suzuki, N. Tamura, H.A. Sakaue, D. Kato, I. Murakami, T. Higashiguchi, LHD Experiment Group, *APL Photon.* **2**, 081301 (2017)
- H. Hara, G. Arai, Y. Kondo, T.-H. Dinh, P. Dunne, G. O’Sullivan, T. Ejima, T. Hatano, W. Jiang, M. Nishikino, A. Sasaki, A. Sunahara, T. Higashiguchi, *Appl. Phys. Express* **9**, 066201 (2016)